

Journal of Applied Sciences

ISSN 1812-5654





Solution Structure and Stability of Fully Developed Thermal Flows Through a Curved Rectangular Duct

¹R.N. Mondal, ²D. Tarafder, ¹M.A. Huda, ¹M. Samsuzzoha and ¹M. Sharif Uddin

¹Mathematics Discipline,

²Computer Science and Engineering Discipline,

Science, Engineering and Technology School, Khulna University, Khulna-9208, Bangladesh

Abstract: Solution structure and stability of fully developed thermal flows through a curved rectangular duct of aspect ratio 2 is investigated numerically by using the spectral method over a wide range of the Dean number $0 \le Dn \le 1000$. A temperature difference is applied across the vertical sidewalls for the Grashof number $1000 \le Gr \le 1500$, where the outer wall is heated and the inner wall is cooled. Though the present study covers a wide range of the Grashof number, in this paper, however, a single case of the Grashof number Gr = 1500 is investigated in detail. First, steady solutions are obtained by the Newton-Raphson iteration method. Linear stability of the steady solutions is then investigated. It is found that among multiple branches of steady solutions obtained, only one branch, which exists throughout whole range of the Dean number, is linearly stable in a couple of interval of Dn while the other branches are linearly unstable. Secondary flow patterns, axial velocity distribution and temperature profile on each of the branches are also obtained.

Key words: Curved rectangular duct, steady solutions, stability, secondary flows, Dean number

INTRODUCTION

The study of flows through a curved duct is of fundamental interest because of its ample applications in fluids engineering, such as in air conditioning systems, refrigeration, heat exchangers, ventilators and the bladeto-blade passages in modern gas turbines. Blood flow in human veins and arteries is another important application of the curved duct flows. The flow through a curved duct shows physically interesting feature under the action of the centrifugal force caused by the curvature of the duct. The presence of curvature generates centrifugal forces which act at right angle to the main flow direction and produce secondary flows. Dean (1927) was the first who formulated the problem in mathematical terms under the fully developed flow condition. He found the secondary flow consisting of a pair of counter rotating vortices caused by the centrifugal force. Since then, there have been a lot of theoretical and experimental works concerning this flow. The readers are referred to Berger et al. (1983), Nandakumar and Masliyah (1986) and Ito (1987) for some outstanding reviews on curved duct flows.

One of the interesting phenomena of the flow through a curved duct is the bifurcation of the flow because generally there exist many steady solutions due to channel curvature. Dennis and Ng (1982), Nandakumar

and Masliyah (1982) and later Yanase et al. (1989) studied dual solutions of the flow through a curved duct. Yang and Keller (1986) studied the bifurcation of the flow for small curvature and found multiple branches of solutions. Thangam and Hur (1990) studied the characteristics of laminar secondary flows in a curved rectangular duct. An early bifurcation structure and linear stability of the steady solutions for fully developed flows in a curved square duct was investigated by Winters (1987). He applied bifurcation analysis to it and found that there are many symmetric and asymmetric steady solutions among which linearly stable ones are few. However, the existence of the multiple solutions of the flow through a curved duct with the large aspect ratio was first studied by Yanase and Nishiyama (1988). They obtained two kinds of solutions: the two-vortex solution and the four-vortex solution for the same aspect ratio. Wang and Yang (2004) performed a numerical study on fully developed bifurcation structure and stability of the forced convection in a curved square duct flow. Very recently, Mondal et al. (2006) performed numerical prediction of thermal flows through a curved square duct and investigated transitional behavior of the unsteady solutions. However, complete bifurcation structure as well as linear stability of the thermal and non-thermal flows through curved ducts with square and rectangular cross sections were performed by Mondal (2006).

One of the most important applications of curved duct flow is to enhance the thermal exchange between two sidewalls, because it is possible that the secondary flow may convey heat and then increases the heat flux between two sidewalls. Chandratilleke and Nursubyakto (2003) presented numerical calculations to describe the secondary flow characteristics in the flow through curved ducts of aspect ratios ranging from 1 to 8 that were heated on the outer wall, where they studied for small Dean numbers and compared the numerical results with their experimental data. Recently, Yanase et al. (2005a) performed numerical investigation of thermal (Gr = 100) and non-thermal flows (Gr = 0) through a curved rectangular duct with differentially heated vertical sidewalls, where they obtained many branches of steady solutions and addressed the time-dependent behavior of the unsteady solutions. Yanase et al. (2005b) studied the bifurcation structure as well as the effects of secondary flows on convective heat transfer for moderate Grashof numbers. However, complete bifurcation structure as well as stability of thermal flows for larger Grashof numbers are yet unresolved, which is important to investigate from both engineering and scientific point of view.

In the present research, a numerical study is presented for the fully developed two-dimensional flow of viscous incompressible fluid through a curved rectangular duct for larger Grashof numbers. Flow characteristics are studied over a wide range of the Dean number by finding the steady solutions and investigating their linear stability. Flow patterns on each of the branches are also obtained.

GOVERNING EQUATIONS

Consider a hydrodynamically and thermally fully two-dimensional flow developed viscous incompressible fluid through a curved duct with a constant curvature. The cross section of the duct is a rectangle with width 2 d and height 2 h. It is assumed that the outer wall of the duct is heated while the inner one is cooled. The temperature of the outer wall is $T_0 + \Delta T$ and that of the inner wall is $T_0 + \Delta T$, where $\Delta T > 0$. The x, y and z axes are taken to be in the horizontal, vertical and axial directions, respectively. It is assumed that the flow is uniform in the z direction and that it is driven by a constant pressure gradient G along the center-line of the duct as shown in Fig. 1.

All the variables are nondimensionalized by using the representative length d, the representative velocity $U_0 = \nu/d$, the representative time $d/U_0 = d^2/\nu$, where ν is

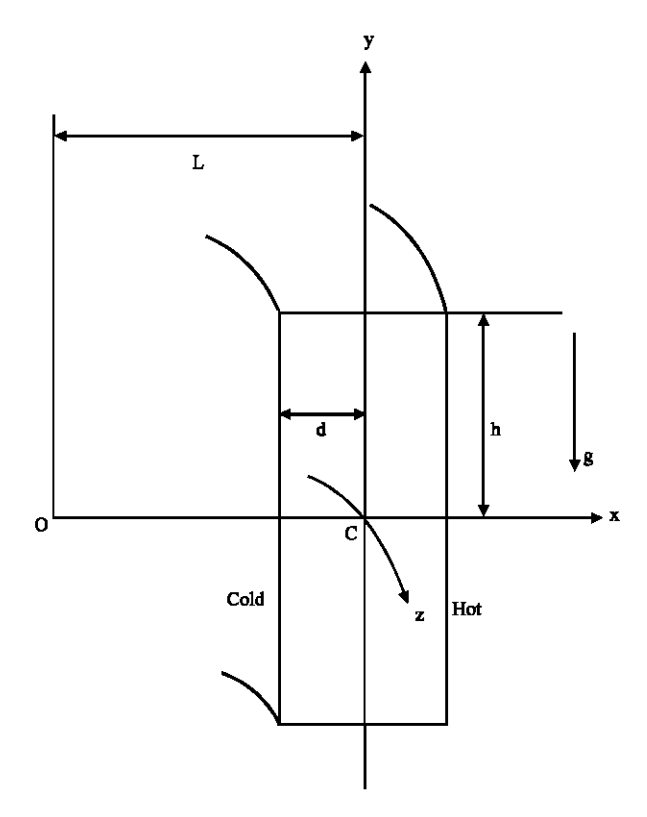


Fig. 1: Coordinate system of the curved rectangular duct

the kinematic viscosity. u, v and w are the velocity components in the x, y and z directions respectively. Velocity components in the x and y directions are nondimensionalized by U_0 and by $U_0/\sqrt{2\delta}$ in the z direction, where $\delta = d/L$ is the curvature of the duct, L is the radius of the duct curvature and temperature is nondimensionalized by ΔT . Henceforth, all the variables are nondimensionalized if not specified. The sectional stream function ψ is introduced as

$$u = \frac{1}{1 + \delta x} \frac{\partial \psi}{\partial y}, \quad v = -\frac{1}{1 + \delta x} \frac{\partial \psi}{\partial x}.$$
 (1)

A new coordinate variable y' is introduced in the y direction as $y = \ell y'$, where $\ell = h/d$ is the aspect ratio of the cross section. From now on, y denotes y' for the sake of simplicity. The basic equations for w, ψ and T are then derived from the Navier-Stokes equations and the energy equation with the Boussinesq approximation as,

$$\begin{split} \left(1+\delta x\right) & \frac{\partial w}{\partial t} + \frac{1}{\ell} \frac{\partial \left(w,\psi\right)}{\partial \left(x,y\right)} - Dn + \frac{\delta^2 w}{1+\delta x} = \left(1+\delta x\right) \Delta_2 w \\ & - \frac{\partial}{\ell \left(1+\delta x\right)} \frac{\partial \psi}{\partial y} w + \delta \frac{\partial w}{\partial x}, \end{split} \tag{2}$$

$$\begin{split} &\left(\Delta_{2} - \frac{\delta}{1 + \delta x} \frac{\partial}{\partial x}\right) \frac{\partial \psi}{\partial t} = -\frac{1}{\ell \left(1 + \delta x\right)} \frac{\partial \left(\Delta_{2} \psi, \psi\right)}{\partial (x, y)} + \frac{\delta}{\ell \left(1 + \delta x\right)^{2}} \\ &\times \left[\frac{\partial \psi}{\partial y} \left(2\Delta_{2} \psi - \frac{3\delta}{1 + \delta x} \frac{\partial \psi}{\partial x} + \frac{\partial^{2} \psi}{\partial x^{2}}\right) - \frac{\partial \psi}{\partial x} \frac{\partial^{2} \psi}{\partial x \partial y}\right] + \frac{\delta}{\left(1 + \delta x\right)^{2}} \\ &\times \left[3\delta \frac{\partial^{2} \psi}{\partial x^{2}} - \frac{3\delta^{2}}{1 + \delta x} \frac{\partial \psi}{\partial x}\right] - \frac{2\delta}{1 + \delta x} \frac{\partial}{\partial x} \Delta_{2} \psi + \frac{1}{\ell} w \frac{\partial w}{\partial y} \\ &+ \Delta_{2}^{2} \psi - Gr \left(1 + \delta x\right) \frac{\partial T}{\partial x}, \end{split} \tag{3}$$

$$\frac{\partial T}{\partial t} + \frac{1}{\ell} \frac{1}{(1 + \delta x)} \frac{\partial (T, \psi)}{\partial (x, y)} = \frac{1}{Pr} \left(\Delta_2 T + \frac{\delta}{1 + \delta x} \frac{\partial T}{\partial x} \right)$$
(4)

where

$$\Delta_{2} = \frac{\partial^{2}}{\partial x^{2}} + \frac{1}{\ell^{2}} \frac{\partial^{2}}{\partial y^{2}}, \quad \frac{\partial (f,g)}{\partial (x,y)} = \frac{\partial f \partial g}{\partial x \partial y} - \frac{\partial f \partial g}{\partial y \partial x}$$
 (5)

The Dean number Dn, the Grashof number Gr and the Prandtl number Pr which appear in Eq. (2) to (4) are defined as

$$Dn = \frac{Gd^3}{\mu\nu} \sqrt{\frac{2d}{L}}, \quad Gr = \frac{\gamma g \Delta T d^3}{\nu^2}, \quad Pr = \frac{\nu}{k}$$
 (6)

where μ , γ , κ and g are the viscosity, the coefficient of thermal expansion, the coefficient of thermal diffusivity and the gravitational acceleration, respectively. The rigid boundary conditions for w and ψ are used as

$$\begin{split} &w(\pm 1,\ y)=w(x,\pm 1)=\psi(\pm 1,y)\\ &=\psi(x,\pm 1)=\frac{\partial \psi}{\partial x}(\pm 1,y)=\frac{\partial \psi}{\partial y}(x,\pm 1)=0, \end{split} \tag{7}$$

and the temperature T is assumed to be constant on the walls as

$$T(1,y)=1$$
, $T(-1,y)=-1$, $T(x,\pm 1)=x$, (8)

NUMERICAL METHOD

In order to solve the Eq. (2) to (4) numerically the spectral method is used. This is the method which is thought to be the best numerical method to solve the Navier-Stokes equations as well as the energy equation (Gottlieb and Orszag, 1977). Detail of this method is discussed in Mondal (2006). By this method the variables

are expanded in a series of functions consisting of the Chebyshev polynomials. That is, $\Phi_{\text{n}}(x)$ and $\Psi_{\text{n}}(x)$ are expressed as

$$\Phi_{n}(x) = (1-x^{2})C_{n}(x), \quad \Psi_{n}(x) = (1-x^{2})^{2}C_{n}(x)$$
 (9)

where

$$C_n(\mathbf{x}) = \cos(n\cos^{-1}(\mathbf{x})) \tag{10}$$

is the nth order Chebyshev polynomial, $w(x,\ y,\ t),$ $\psi(x,\ y,\ t)$ and $T(x,\ y,\ t)$ are expanded in terms of the expansion functions $\Phi_{n}(x)$ and $\Psi_{n}(x)$ as

$$\begin{split} w(x,y,t) &= \sum_{m=0}^{M} \sum_{n=0}^{N} w_{mn}(t) \Phi_{m}(x) \Phi_{n}(y), \\ \psi(x,y,t) &= \sum_{m=0}^{M} \sum_{n=0}^{N} \Psi_{mn}(t) \Psi_{m}(x) \Psi_{n}(y), \\ T(x,y,t) &= \sum_{m=0}^{M} \sum_{n=0}^{N} T_{mn}(t) \Phi_{m}(x) \Phi_{n}(y) + x \end{split}$$
 (11)

where M and N are the truncation numbers in the x and y directions, respectively. The expansion coefficients w_{mn} , ψ_{mn} and T_{mn} are then substituted into the basic Eq. 2-4 and the collocation method is applied. As a result, the nonlinear algebraic equations for w_{mn} , ψ_{mn} and T_{mn} are obtained. The collocation points are taken to be

$$x_{i} = \cos\left[\pi\left(1 - \frac{i}{M+2}\right)\right], \quad i = 1,..., M+1$$

$$y_{j} = \cos\left[\pi\left(1 - \frac{j}{N+2}\right)\right], \quad j = 1,..., N+1$$
(12)

The steady solutions are then obtained by the Newton-Raphson iteration method assuming that all the coefficients are time independent. The convergence is assured by taking $\epsilon_{\rm p} < 10^{-10}$, where subscript p denotes the iteration number and $\epsilon_{\rm p}$ is defined as

$$\epsilon_{p} = \sum_{m=0}^{M} \sum_{n=0}^{N} \left[\left(w_{mn}^{(p+1)} - w_{mn}^{p} \right)^{2} + \left(\psi_{mn}^{(p+1)} - \psi_{mn}^{p} \right)^{2} + \left(T_{mn}^{(p+1)} - T_{mn}^{p} \right)^{2} \right].$$

In the present numerical calculations, M=20 and N=40 have been used for sufficient accuracy of the solutions. Numerical calculations are carried out for the curvature $\delta=0.1$ over a wide range of the Dean number $0 \le Dn \le 1000$ for the Grashof number $1000 \le Gr \le 1500$ for $\ell=2$.

RESISTANCE COEFFICIENT

In the present study, the resistance coefficient λ is used as the representative quantity of the flow state. It is also called the hydraulic resistance coefficient and is generally used in fluids engineering, defined as

$$\frac{P_{1}^{*} - P_{2}^{*}}{\Delta z^{*}} = \frac{\lambda}{d_{h}^{*}} \frac{1}{2} \rho \left\langle w^{*} \right\rangle^{2}$$
 (13)

where quantities with an asterisk denote dimensional ones, $\langle \ \rangle$ stands for the mean over the cross section of the rectangular duct, ρ the density and $d_h^* = 4(2d\times 2d\ell)/(4d\times 4d\ell)$ is the hydraulic diameter. The mean axial velocity $\langle w^* \rangle$ is calculated by

$$\left\langle \mathbf{w}^{*}\right\rangle = \frac{v}{4\sqrt{2\delta}d} \int_{-1}^{1} d\mathbf{x} \int_{-1}^{1} \mathbf{w}\left(\mathbf{x}, \mathbf{y}, \mathbf{t}\right) d\mathbf{y} \tag{14}$$

Since $(P_1^*-P_2^*)/\Delta z^* = G$, λ is related to the mean non-dimensional axial velocity $\langle w \rangle$ as

$$\lambda = \frac{8\ell\sqrt{28}Dn}{(1+\ell)\langle w \rangle^2},\tag{15}$$

where

$$\langle w \rangle = \sqrt{2\delta} d \langle w^* \rangle / v \cdot$$

In the present study, λ is used to denote the steady solution branches.

RESULTS AND DISCUSSION

Solution structure and steady solutions: We obtain five branches of asymmetric steady solutions over a wide range of the Dean number $0 \le Dn \le 1000$ for the Grashof number $1000 \le Gr \le 1500$. Figure 2 and 3a show solution structures of the steady solutions for Gr = 1000 and Gr = 1500, respectively. As seen in Fig. 2 and 3a, the bifurcation structures are topologically nearly similar for any Gr in the range. Therefore, in the present study, a single case of the Grashof number Gr = 1500 will be discussed in detail. The steady solutions are obtained by the path continuation technique with different initial guesses as discussed by Mondal (2006). Figure 3a shows bifurcation structure of the steady solutions for Gr = 1500 and $100 \le Dn \le 1000$ using λ , the representative quantity

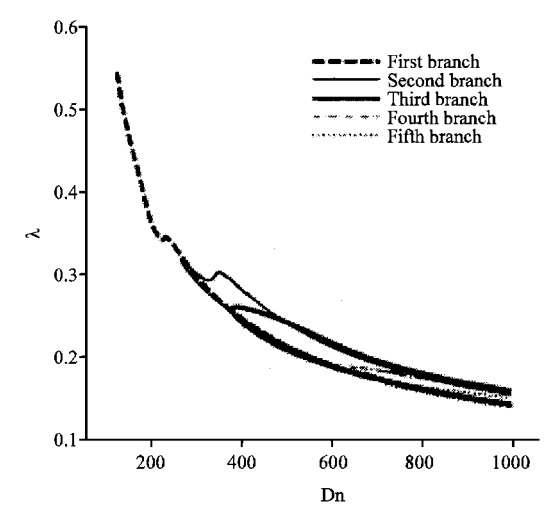


Fig. 2: Steady solution branches for Gr = 1000 and $100 \le Dn \le 1000$

of the solutions. The steady solution branches are named the first steady solution branch (first branch, long dashed line), the second steady solution branch (second branch, thin solid line), the third steady solution branch (third branch, thick solid line), the fourth steady solution branch (fourth branch, dash dotted line) and the fifth steady solution branch (fifth branch, dotted line), respectively. In order to see the intricate branch structure as well as to distinguish the steady solution branches from each other, an enlargement of Fig. 3a is shown in Fig. 3b at larger Dean numbers, where it is seen that the steady solution branches are independent and there exists no bifurcating relationship among the branches in the parameter range investigated in this study. However, some branches overlap at larger Dean numbers but they represent different branches as discussed later. The solution branches are distinguished by the nature and number of secondary flow vortices appearing in the cross section of the duct. In this regard, it should be remarked that Yanase et al. (2005a) obtained both symmetric and asymmetric steady solutions for the non-thermal flow in a curved rectangular duct. In the present study of thermal flows, however, we obtain only asymmetric steady solutions. The reason is that heating the outer wall causes deformation of the secondary flow and yields asymmetry of the flow. In the following, the steady solution branches as well as flow patterns on the respective branches are discussed.

The first steady solution branch: The first steady solution branch for Gr = 1500 is solely depicted in Fig. 4a for $10 \le Dn \le 1000$. It should be remarked here that

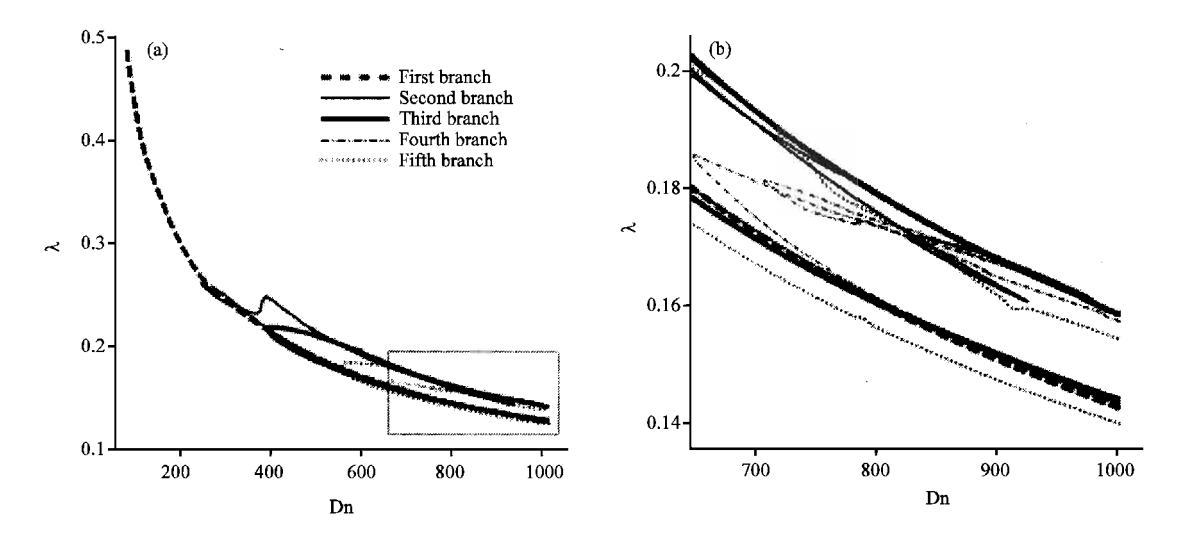


Fig. 3: (a) Steady solution branches for Gr = 1500 and $100 \le Dn \le 1000$, (b) Enlargement of (a) at larger Dean numbers $(660 \le Dn \le 1000)$

among five branches of steady solutions, this is the only branch which exists throughout the whole range of the Dean number. As seen in Fig. 4a, the first branch starts from point a (Dn = 10) and goes to the direction of increasing Dn and decreasing λ up to point c (Dn = 1000) without turning on its way. To observe the change of the flow patterns and temperature distributions, contours of typical secondary flow, axial velocity and temperature profile on the first branch are shown in Fig. 4b for several values of Dn, where the contours of ψ , w and T are drawn with the increments $\Delta \psi = 0.6$, $\Delta w = 10$ and $\Delta T = 0.2$, respectively. The same increments of ψ , w and T are used for all the figures in this paper, if not specified. The righthand side of each duct box of ψ , w and T is in the outside direction of the duct curvature. In the figures of the secondary flow, solid lines $(\psi \ge 0)$ show that the secondary flow is in the counter clockwise direction while the dotted lines ($\psi < 0$) in the clockwise direction. Similarly, in the figures of the temperature field, solid lines are those for $T \ge 0$ and dotted ones for T<0. As seen in Fig. 4b, the first branch contains one- and two-vortex solutions which are asymmetric with respect to the horizontal center plane y = 0. Heating the outer wall causes deformation of the secondary flow and yields asymmetry of the flow. With the heating and cooling the sidewalls, changes to fluid density induce thermal convection. The resulting flow behavior in the cross section is, therefore, determined by the combined action of the radial flow caused by the centrifugal body force and the convection by the temperature difference. At smaller Dean numbers, the centrifugal body force is weaker and the thermal convection dominates the flow;

the resulting flow consists of a single vortex, which occupies the entire cross section. At larger Dean numbers, on the other hand, the centrifugal body force becomes stronger and the secondary flow is gradually reestablished. In this study, the name number-vortex solution is used when the number of secondary vortices is clearly counted, since such kind of naming is commonly used in this field of study. As seen in Fig. 4b, maximum axial velocity is shifted near the outer bend of the duct as Dn increases.

The second steady solution branch: The second steady solution branch, shown by a thin solid line in Fig. 3a, is solely depicted in Fig. 5a for $250 \le Dn \le 1000$. The branch is comparatively entangled than other branches with many turning points throughout its way. As seen in Fig. 5a, the branch starts from point a at larger Dean number (Dn = 1000) and goes to the direction of increasing λ as Dn decreases and turns smoothly at point b (Dn = 262.12). The branch then goes to the direction of increasing Dn and decreasing λ up to point c where it turns again to increasing λ and arrives at point d. The branch then extends to the direction of increasing Dn and decreasing λ and finally arrives at point I (Dn = 1000) with turning on its way at points e, f, g and h. Contours of secondary flow, axial velocity and temperature profile at several values of Dn on this branch are shown in Fig. 5b. It is found that the secondary flow is a two-vortex solution from point a to point b (Dn decreases), but on the route from point b down to point I an additional pair of secondary vortices appear in the central part of the righthand side of the duct cross section. These additional

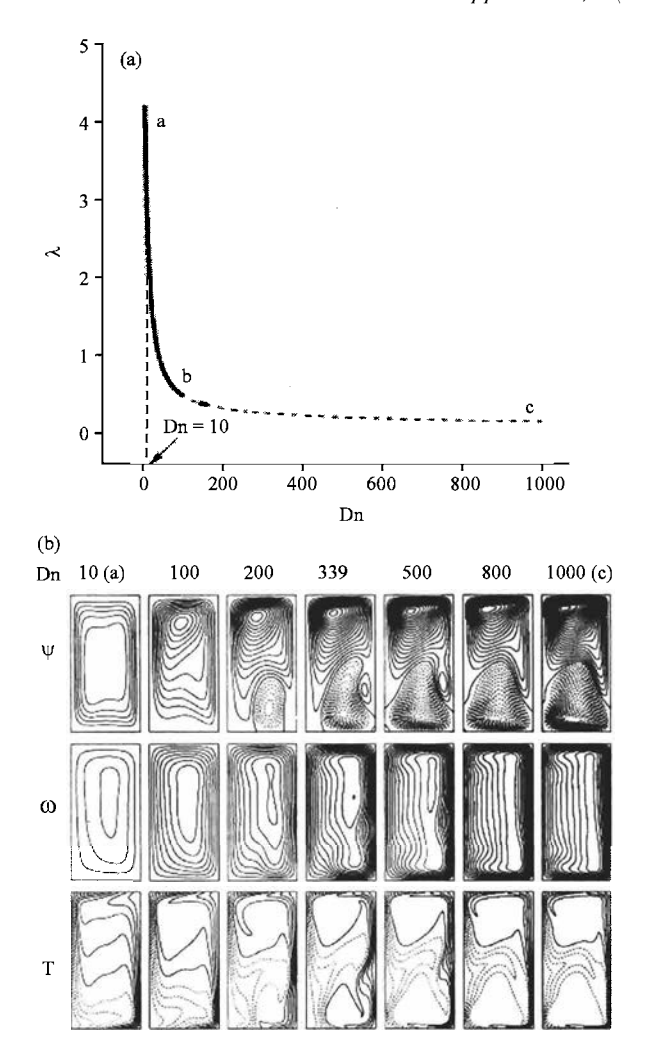
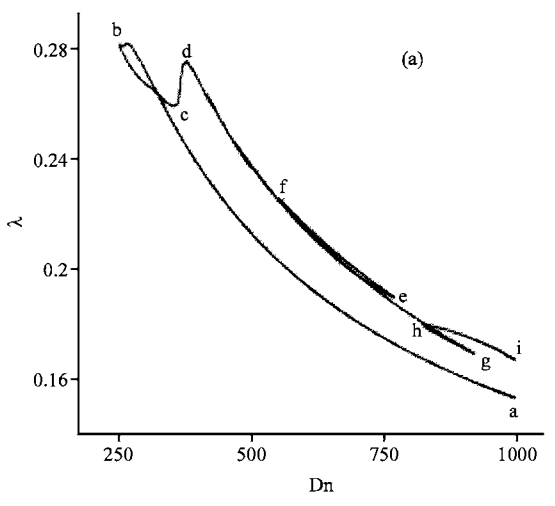


Fig. 4: (a) First steady solution branch with the region of linear stability (solid bold line) for Gr = 1500. (b) Contours of secondary flow (top), axial velocity (middle) and temperature profile (bottom) for the first steady solution branch

vortices are called Dean vortices which play an important role in the enhancement of heat transfer. As seen in Fig. 5b, the maximum axial velocity is shifted near the outer wall of the duct and as the secondary flow is strengthened (i.e., Dn increases), the region of the axial velocity is separated into two high velocity regions.

The third steady solution branch: The third steady solution branch, shown by a thick solid line in Fig. 3a, is exclusively depicted in Fig. 6a. As seen in Fig. 6a, the branch starts from point a (Dn = 1000) and goes to the direction of decreasing Dn as λ becomes large and turns smoothly at point b (Dn = 400.08). The branch then goes to the direction of increasing Dn and decreasing λ which extends up to point d (Dn = 1000) without further turning



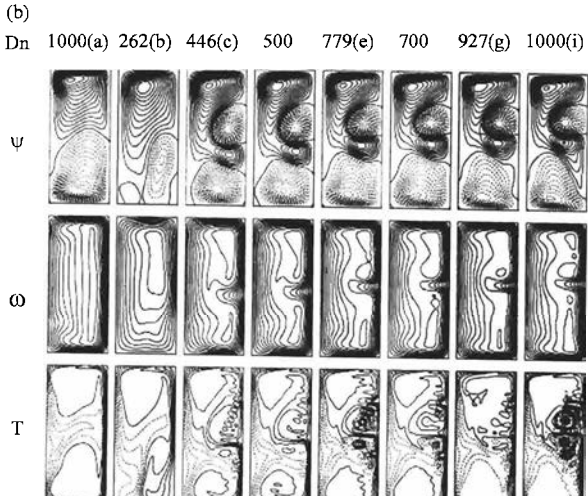


Fig. 5: (a) Second steady solution branch for Gr = 1500. (b) Contours of secondary flow (top), axial velocity (middle) and temperature profile (bottom) for the second steady solution branch

on its way. We show the secondary flow patterns, axial velocity distribution and temperature profiles at several values of Dn on this branch in Fig. 6b. It is found that the third branch starts with a two-vortex solution at point a and becomes a four-vortex solution at point b which remains a four-vortex solution up to point c. As seen in Fig. 6b, the maximum axial velocity is pushed near the outer wall of the duct due to strong centrifugal force as Dn increases.

The fourth steady solution branch: The fourth steady solution branch is shown in Fig. 7a. As seen in Fig. 7a, the branch exists only for larger Dean numbers (650 \leq Dn \leq 1000) and a little bit complex like the second branch with some turning points on its way. The branch starts from point a (Dn = 1000) and goes to the direction of increasing λ as Dn decreases and experiences a gentle turning at

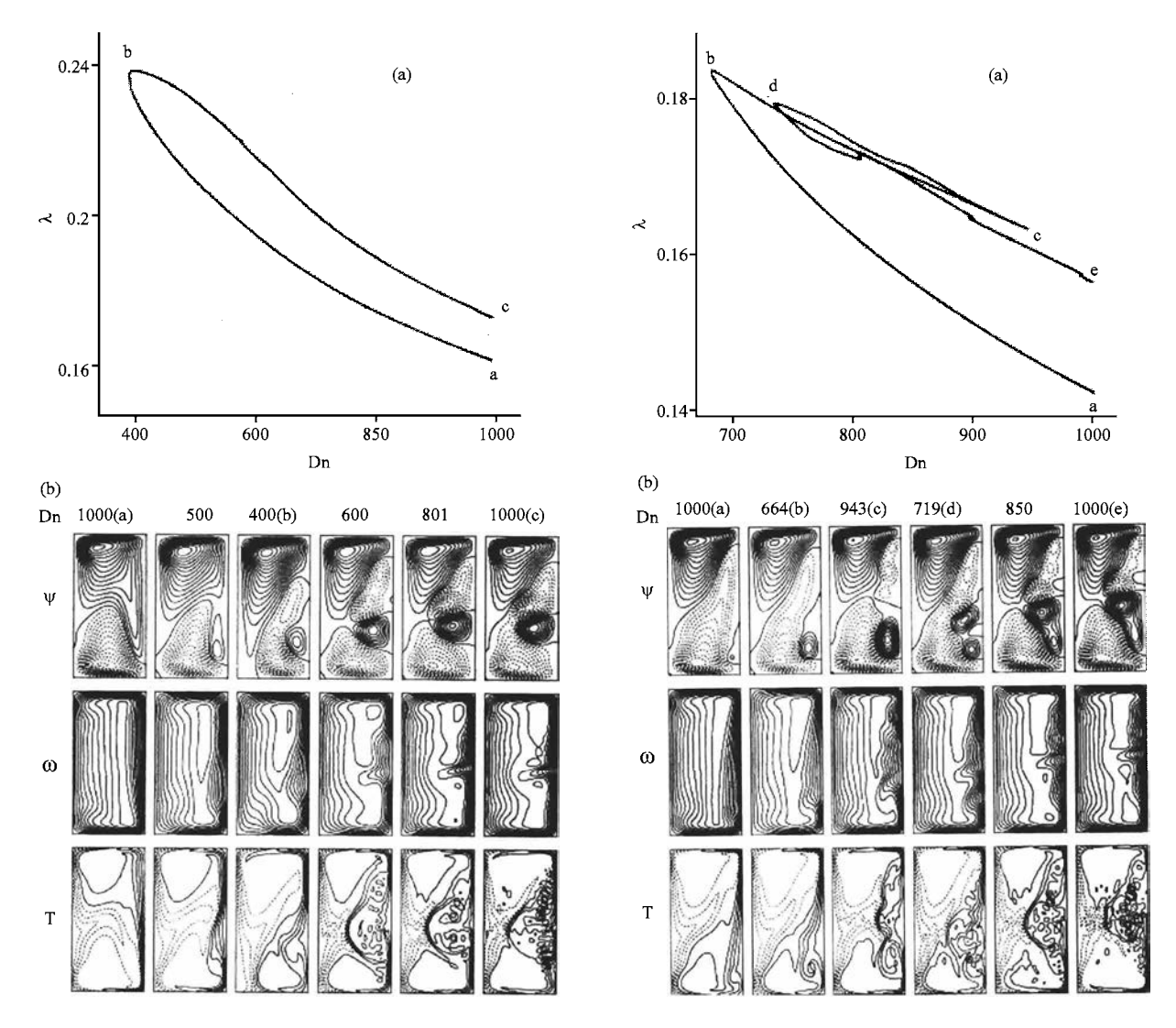


Fig. 6: (a) Third steady solution branch for Gr = 1500. (b) Contours of secondary flow (top), axial velocity (middle) and temperature profile (bottom) for the third steady solution branch

Fig. 7: (a) Fourth steady solution branch for Gr = 1500. (b) Contours of secondary flow (top), axial velocity (middle) and temperature profile (bottom) for the fourth steady solution branch

point b (Dn = 664.15) in the opposite direction. The branch then goes to the direction of increasing Dn and decreasing λ up to point c (Dn = 943.07), where it turns again to the opposite direction up to point d (Dn = 719.20). The branch finally arrives at point e (Dn = 1000) extending in the direction of increasing Dn and decreasing λ with some gentle turning on its way. To observe the change of the flow characteristics, contours of secondary flow, axial velocity and temperature profile at several values of Dn on this branch are shown in Fig. 7b, where it is seen that the secondary flow is a two-, four-, six- and eight-vortex solution. As seen in Fig. 7b, the maximum axial velocity is shifted near

the outer wall of the duct and the region of the axial velocity is separated into several high velocity regions with increasing Dn. Temperature distribution is also vigorous as the secondary flow becomes strong.

The fifth steady solution branch: The fifth steady solution branch, shown by a dotted line in Fig. 3a, is solely depicted in Fig. 8a. As seen in Fig. 8a, the path of the branch is gentle like the third branch. It starts from point a (Dn = 1000) and goes to the direction of increasing λ as Dn becomes small and turns smoothly at point b (Dn = 553.10). The branch then goes to the direction of increasing Dn and decreasing λ and extends up to point

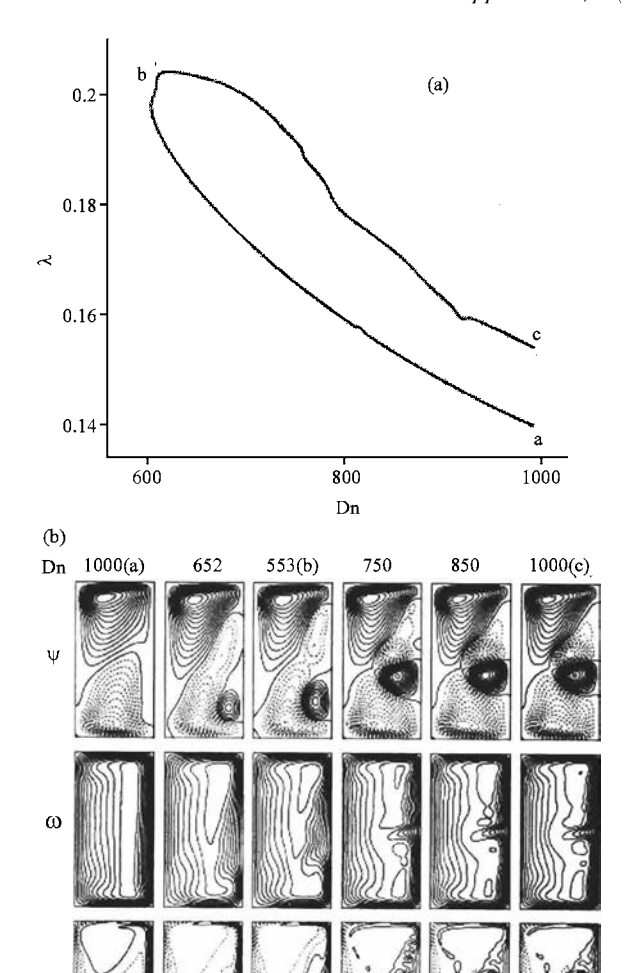


Fig. 8: (a) Fifth steady solution branch for Gr = 1500. (b) Contours of secondary flow (top), axial velocity (middle) and temperature profile (bottom) for the fifth steady solution branch

d (Dn = 1000). We show the secondary flow patterns, axial velocity distribution and temperature profiles at several values of Dn on this branch in Fig. 8b. As seen in Fig. 8b, the branch is composed of two-, four- and sixvortex solutions. Maximum axial velocity is pushed near the outer wall as Dn increases and the temperature distribution is strengthened as the secondary vortices become stronger.

Linear stability of the steady solutions: In this paper, we examine linear stability of the steady solutions against only two dimensional (z-independent) perturbations. To do this, the eigenvalue problem is solved which is constructed by the application of the function expansion

Table 1: Linear stability of the first steady solution branch for Gr = 1500			
Dn	λ	$\sigma_{_{\scriptscriptstyle T}}$	σ_{i}
0	0.000000	-9.1317×10 ^{−1}	0
50	0.961439	-9.5462×10 ⁻¹	0
100	0.539385	-9.2673×10 ⁻¹	0
105	0.520232	-2.6418×10^{-2}	± 8.085
106	0.516602	4.0481×10^{-2}	± 7.957
125	0.457146	3.5542	± 2.818
143	0.421276	6.3946×10^{-2}	$\pm 7.957 \times 10$
144	0.419762	-3.8057×10^{-2}	$\pm 1.185 \times 10$
165	0.389955	-1.1998×10 ⁻²	$\pm 1.464 \times 10$
166	0.388609	4.2156×10 ⁻²	$\pm 1.469 \times 10$
300	0.277386	1.0757×10	± 5.204
500	0.212141	2.3176×10	± 2.791
1000	0.143013	5.9401×10	±4.445×10

method together with the collocation method to the perturbation equations obtained from Eq. (2-4). It is assumed that the time dependence of the perturbation is $e^{\sigma t}$, where $\sigma = \sigma_r + i\sigma_i$ is the eigenvalue with σ_r the real part, σ_i the imaginary part and $\frac{1}{i} = \sqrt{-1}$. If all the real parts of the eigenvalue σ are negative, the steady solution is linearly stable, but if there exists at least one positive real part of the eigenvalue, it is linearly unstable. In the unstable region, the perturbation grows monotonically for $\sigma_i = 0$ and oscillatorily for $\sigma_i \neq 0$.

On the basis of the above-mentioned criteria, linear stability of the steady solutions is investigated. It is found that among five branches of steady solutions, only the first branch, which exists throughout the whole range of the Dean number, is linearly stable in a couple of interval of Dn, while the other branches are linearly unstable. The eigenvalues of the first steady solution branch are listed in Table 1 where the eigenvalues with the maximum real part of σ are presented. Those for the linearly stable solutions are printed in bold letters. As seen in Table 1, the stability region exists for $0 \le Dn \le 105$ and $144 \le Dn \le 165$ and the perturbation grows oscillatorily $(\sigma_i \neq 0)$ for Dn \geq 105. Therefore, the Hopf bifurcation occurs at Dn ≈ 105. Linearly stable steady solution regions are shown with thick solid lines in Fig. 4a.

Phase diagram of the steady solutions: Finally, the distribution of the steady two-, four-, six- and eight-vortex solutions, obtained at different values of the Dean number on the multiple branches, is shown in Fig. 9 in the Dean number vs. stream function plane (Dn- ψ plane) for $0 \le Dn \le 1000$, where the regions of different solutions are displayed with shading surrounded by solid boundaries. In this picture, the vortices are represented by different symbols. In this study, it is found that only two-vortex solutions are generated for small Dn's. However, as Dn is increased gradually, the number of vortices also increases. We obtain two-vortex solutions for $0 \le Dn \le 262$, two- and four-vortex solutions for $262 < Dn \le 720$

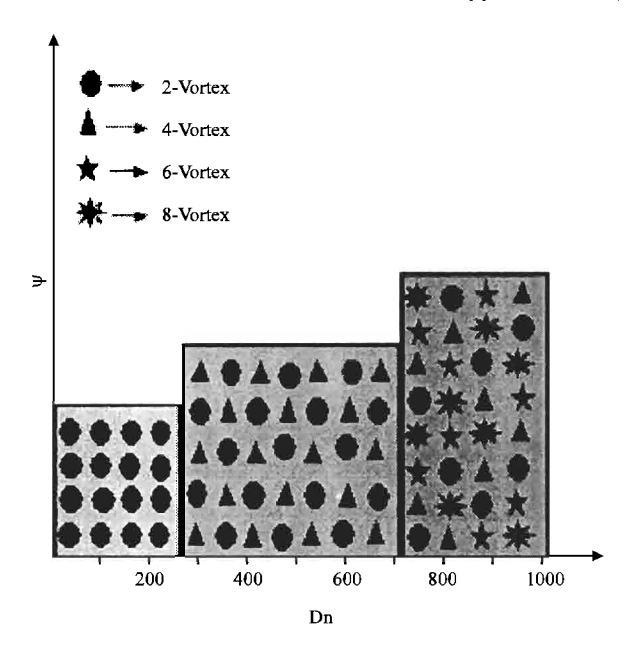


Fig. 9: Phase diagram of the steady solutions for Gr = 1500

and two-, four-, six- and eight-vortex solutions for Dn > 720. Thus from Fig. 9 we obtain a quick knowledge about the flow structure for Gr = 1500.

REFERENCES

- Berger, S.A., L. Talbot and L.S. Yao, 1983. Flow in curved pipes. Ann. Rev. Fluid. Mech., 35: 461-512.
- Chandratilleke, T.T. and Nursubyakto, 2003. Numerical prediction of secondary flow and convective heat transfer in externally heated curved rectangular ducts. Int. J. Thermal Sci., 42: 187-198.
- Dean, W.R., 1927. Note on the motion of fluid in a curved pipe. Philos. Mag., 4: 208-223.
- Dennis, S.C.R. and M. Ng, 1982. Dual solutions for steady laminar flow through a curved tube. Quart. J. Mech. Applied Math., 35: 305-324.
- Gottlieb, D. and S.A. Orszag, 1977. Numerical analysis of spectral methods. Society for Industrial and Applied Mathematics, Philadelphia.
- Ito, H., 1987. Flow in curved pipes. JSME Int. J., 30: 543-552.

- Mondal, R.N., 2006. Isothermal and non-isothermal flows through curved ducts with quare and rectangular cross sections. Ph.D. Thesis, Okayama University, Japan.
- Mondal, R.N., Y. Kaga, T. Hyakutake and S. Yanase, 2006. Effects of curvature and convective heat transfer in curved square duct flows. Trans. ASME., J. Fluids Eng., 128: 1013-1023.
- Nandakumar, K. and H.J. Masliyah, 1982. Bifurcation in steady laminar flow through curved tubes. J. Fluid Mech., 119: 475-490.
- Nandakumar, K. and J.H. Masliyah, 1986. Swirling flow and heat transfer in coiled and twisted pipes. Adv. Transport Process., 4: 49-112.
- Thangam, S. and N. Hur, 1990. Laminar secondary flows in curved rectangular ducts. J. Fluid Mech., 217: 421-440.
- Wang, L. and T. Yang, 2004. Bifurcation and stability of forced convection in curved ducts of square cross section. Int. J. Heat Mass Transfer, 47: 2971-2987.
- Winters, K.H., 1987. A bifurcation study of laminar flow in a curved tube of rectangular cross-section. J. Fluid Mech., 180: 343-369.
- Yanase, S. and K. Nishiyama, 1988. On the bifurcation of laminar flows through a curved rectangular tube. J. Phys. Soc. Japan, 57: 3790-3795.
- Yanase, S., N. Goto and K. Yamamoto, 1989. Dual solutions of the flow through a curved tube. Fluid Dyn. Res., 14: 191-201.
- Yanase, S., R.N. Mondal, Y. Kaga and K. Yamamoto, 2005a. Transition from steady to chaotic states of isothermal and non-isothermal flows through a curved rectangular duct. J. Phys. Soc. Japan, 74: 345-358.
- Yanase, S., R.N. Mondal and Y. Kaga, 2005b. Numerical study of non-isothermal flow with convective heat transfer in a curved rectangular duct. Int. J. Thermal Sci., 44: 1047-1060.
- Yang, Z. and H.B. Keller, 1986. Multiple laminar flows through curved pipes. Applied Numerical Math., 2: 257-271.